Fang *et al. Micro and Nano Syst Lett (2017) 5:10*
DOI 10.1186/s40486-017-0044-z

Micro and Nano Systems Letters

LETTER Open Access

Study on high throughput nanomanufacturing of photopatternable nanofibers using tube nozzle electrospinning with multi-tubes and multi-nozzles

Sheng-Po Fang[1*], PitFee Jao[1], David E. Senior[1,2], Kyoung-Tae Kim[1,3] and Yong-Kyu Yoon[1*]

Abstract

High throughput nanomanufacturing of photopatternable nanofibers and subsequent photopatterning is reported. For the production of high density nanofibers, the tube nozzle electrospinning (TNE) process has been used, where an array of micronozzles on the sidewall of a plastic tube are used as spinnerets. By increasing the density of nozzles, the electric fields of adjacent nozzles confine the cone of electrospinning and give a higher density of nanofibers. With TNE, higher density nozzles are easily achievable compared to metallic nozzles, e.g. an inter-nozzle distance as small as 0.5 cm and an average semi-vertical repulsion angle of 12.28° for 8-nozzles were achieved. Nanofiber diameter distribution, mass throughput rate, and growth rate of nanofiber stacks in different operating conditions and with different numbers of nozzles, such as 2, 4 and 8 nozzles, and scalability with single and double tube configurations are discussed. Nanofibers made of SU-8, photopatternable epoxy, have been collected to a thickness of over 80 μm in 240 s of electrospinning and the production rate of 0.75 g/h is achieved using the 2 tube 8 nozzle systems, followed by photolithographic micropatterning. TNE is scalable to a large number of nozzles, and offers high throughput production, plug and play capability with standard electrospinning equipment, and little waste of polymer.

Keywords: SU-8 nanofibers, Lithographically patterned nanofibers, Tube nozzle electrospinning, High throughput, Multijet electrospinning, Large area electrospinning

Background

In the last decade, electrospinning has seen its growth in multiple fields such as biomedical engineering, energy storage, and electronics [1, 2]. Applications using electrospun nanofibers include gas sensors, nerve guidance scaffolds, air filters, nano sensors, energy storage capacitors and solar cells [3–8]. A typical production rate of the electrospun nanofibers using a single spinneret is 0.01–0.1 g/h, which may be appropriate for lab usage or small scale experiments, but not for large scale usage and production [9]. Techniques to produce high throughput nanofibers have been studied by scaling up the spinneret count [10, 11]. Multiple spinnerets can be implemented by using an array of metallic needles either in a linear [12] or a circular [13] array. Although the multiple metallic needle approach gives a production rate of 0.024 g/h per nozzle which is comparable to the single needle production rate [13], the metallic spinnerets are bulky, difficult to assemble, and expensive. To implement non-metallic jetting sources, Dosunmu et al. [14] have used a highly porous reservoir and a conductive wire to charge the polymer. While the technique gives a high production rate of 5 g/h, it shows a wide distribution of nanofiber diameters. By drilling holes half-way through the porous walls, Varabhas et al. [15] have improved the diameter uniformity but lowered the production rate to 0.3 g/h and increased the operating voltages to 60 kV. Using microfluidic channels, Srinivasta et al. [16] have demonstrated intricate janus architecture nanofibers, but

*Correspondence: sfang@ufl.edu; ykyoon@ece.ufl.edu
[1] Electrical and Computer Engineering, University of Florida, 225 Larsen Hall, Gainesville, FL 32611-6200, USA
Full list of author information is available at the end of the article

the open channel approach has lowered throughput to 0.1 g/h with 8 nozzles. Also, drilled holes in plastic films [17] and drilled holes into syringe filters [18] have been reported. But these approaches suffer from non-uniformity in nanofiber diameter or not quite scalable.

Electrospinning of photopatternable polymers allows for direct patterning of the nanofibers using UV lithography of the nanofibers. Norbornene based co-polymer PN3TMA6 with photocrosslinkable units (methacrylate) [19] and Polyethylene oxide (PEO) with photo initiator (Irgacure) in hyaluronic acid [20] have been reported. Recently, multiple groups including the author group have reported on electrospinning and subsequent photopatterning using commercially available SU-8 [7, 21–24]. Patterned nanofibers have been subsequently carbonized after thermal treatment, resulting in good electrodes for high density energy storage devices such as supercapacitors [7, 21, 22]. While the process has large commercial implications in context of nanomanufacturing, so far only a single spinneret approach has been exercised. Recently, the authors have presented the tube nozzle electrospinning (TNE) process [8]. In this paper, the TNE process is described in detail as a high throughput nanofiber fabrication process using a commercially available photopatternable epoxy SU-8 and the photolithographical patterning of the SU-8 nanofibers is detailed. In TNE, low density polyethylene (LDPE) tubes are adopted and a linear nozzle array has been formed using a computer numerical control (CNC) printed circuit board (PCB) milling machine. The semi vertical angle due to electrostatic repulsion between nozzles, the nanofiber diameter, the nanofiber production throughput and the growth rate as a function of the nozzle count, and photopatterning the electrospun nanofiber stacks are detailed.

Experimental

Electrospinning setup: SNE and TNE

Figure 1a shows the conventional single needle electrospinning (SNE) system. The prepared polymer solution is loaded into the syringe without the introduction of bubbles and capped with a 21 gauge stainless steel hypodermic needle (CML Supply LLC, USA). The syringe is then loaded into the syringe pump (NE-1000, New Era Pump Systems Inc.) and programmed to pump at a specified rate. Polymer solution is then charged via the metallic needle tip with a high voltage supply (603C-300P, Spellman High Voltage Electronic Co.). Electrospinning is performed inside a custom fabricated acrylic box for controlled humidity and minimal interference of air-flow from the environment. All experiments are performed at room temperature.

The tube nozzle electrospinning (TNE) setup is shown in Fig. 1b. The stainless steel needle is substituted with the milling-machined tube nozzle and the rest electrospinning equipment remains the same. Figure 2 shows an array of low density polyethylene (LDPE) tubes with an outer diameter of 0.187″, an inner diameter of 0.125″, and a wall thickness of 0.031″ (Value Plastics Inc.) secured on a substrate board so the nozzle holes can be precisely machined on one side of the tube using a PCB milling machine (ProtoMat S100, LPKF Laser & Electronics AG, Germany). A nozzle diameter of 0.2 mm is used in this work. One end of the tube is thermally sealed to implement a closed system and to control the pressure inside the tube. The other end is connected with a luer lock connector (Value Plastics Inc.), allowing it to form easy plug and play connectivity with the standard syringe. A copper wire which connects to the positive power supply is then inserted into the tube on the opposite side of the nozzles to provide electrons to the polymer solution and the entrance into the tube is sealed with epoxy. By coupling two tubes with embedded nozzles, a multi-TNE setup can be achieved to give increased throughput production of nanofibers as shown in Fig. 1c. Increased tube counts require a linear increase in polymer input flow rate. Keeping a fixed distance, the

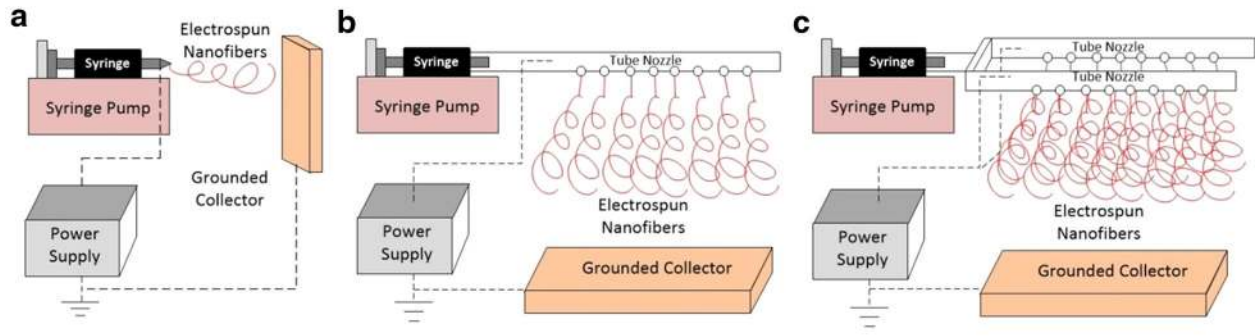

Fig. 1 Schematic of different electrospinning systems: **a** conventional single syringe electrospinning, and tube nozzle electrospinning with (**b**) single tube and **c** dual tubes. All systems accommodate a precision syringe pump, a high voltage source and a grounded collector

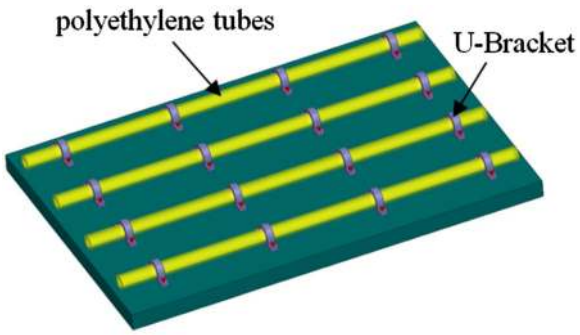

Fig. 2 Diagram of polyethylene tubes secured to a printing circuit board to precisely drill nozzles

voltage is also required to increase to achieve the same electrospinning conditions.

SU-8 2025 (Microchem Inc.) has an intrinsic viscosity of 4500 cSt with a solid content percentage of 68.45%. SU-8 2025 is optimized for the electrospinning process by diluting it in cylcopentanone (Sigma Aldrich Inc.) to reduce the solid content percentage down to 60.87%. The solution is stirred overnight using a magnetic stirring bar and stored in dark amber bottles.

The multiple intermittent electrospinning technique [10, 21] is used in this work to reduce charge accumulation and nanofiber repulsion effects. The electric charge can accumulate inside the collected nanofiber without sufficient resting time, which can limit the nanofiber stack height by repelling the incoming charged nanofiber during electrospinning. In this work, each cycle has 30 s of electrospinning and 30 s of resting to maximize the nanofiber stack height.

Figure 3a shows an electrostatic field distribution simulation of the 8 nozzle TNE by COMSOL Multiphysics 4.3 (COMSOL Inc.). Gradient electric fields indicate the flow of charged particles from the ionized polymer solution to the grounded collector at the bottom. The nozzles are spaced 0.5 cm apart and the tip to collector distance (TCD) is set to 12.5 cm. The divergent trajectory for the electrospun nanofibers results in the increasing in-plane angle of divergence for the nozzles further from the midpoint of the tube. This is attributed to the divergent fields of adjacent jets of charged particles which increase when they are the further away from the jetting source. By adding an additional adjacent tube, similar divergence is observed as that of a single tube except that in the case of two tubes, out-of-plane spatial repulsion in addition to the divergence occurs due to adjacent nozzles as shown in Fig. 3b. The out-of-plane divergence between the tubes is similar to that at the other edges of a single tube. This is attributed to the lack of convergent field as seen by the inner nozzles of a single tube.

Results and discussion

Taylor cone formation and electric repulsion

Operating conditions for SU-8 electrospinning is optimized with a needle voltage of 12.5 kV, a tip-to-collector distance (TCD) of 12.5 cm, and a flow rate of 0.2 ml/min for the SNE approach. In the case of TNE, the increasing nozzle count requires increasing flow rate to continuously replenish the receding droplet during the electrospinning process. Therefore, in the case of 2, 4 and 8 nozzles, the required flow rates are 0.4, 0.8 and 1.6 ml/min, respectively. It is noticed that sorely increasing flow rate without optimizing other operation parameter is insufficient to initiate the electrospinning process. With a TCD of 10 cm, the voltages required for 2, 4, and 8 nozzle TNE to observe the Taylor cone formation and initiate the electrospinning process are 12.5, 15, and 20 kV, respectively. Figure 4a, b shows the Taylor cone formation of 4 and 8 nozzle TNE, respectively. Figure 4c shows electrospinning using 2 tubes with 3 nozzles each and requires a higher needle voltage of 25 kV feeding both the tubes. The Taylor cone is seen to diverge not only between adjacent nozzles but also between adjacent tubes as expected.

Followed by the Taylor cone formation at every nozzle, the polymer droplet quickly shrinks to a very fine jet and elongates until it follows a bending instability stage where the nanofibers are chaotically whipped toward the collector and forming the nanofibers membrane. Table 1 shows the semi-vertical angles (SVA), which are the vertex angles of the electrospinning cone taken for 2, 4 and 8 nozzle architectures. Note that the nozzle number corresponds to that used in Fig. 4. The 2 nozzle architecture shows the highest SVAs when compared to the 4 and 8 nozzle ones. This is attributed to the increased charge repulsion between the two electrospinning cones from closely located nozzles. In the case of the 4 nozzles, while the outer nozzles #1 and #4 have similar SVAs as those of the 2 nozzles, the inner nozzles #2 and #3 have reduced SVAs. A similar trend is observed in the case of 8 nozzle TNE wherein the inner nozzles #3 thru #6 observe even reduced SVAs when compared to those of the 4 nozzle one. It is noticeable that the average SVA (12.28°) of the 8-nozzle architecture measured for an inter-nozzle distance (IND) of 0.5 cm is considerably less than the SVA (30.22°) measured for the linear metallic needle architecture with an IND of 4 cm [13]. The density of nozzles achieved with the TNE architecture is almost an order of magnitude higher than that of the metallic needle architecture. This allows a higher density of nanofibers to be collected per unit area of a substrate for the given nozzle architecture.

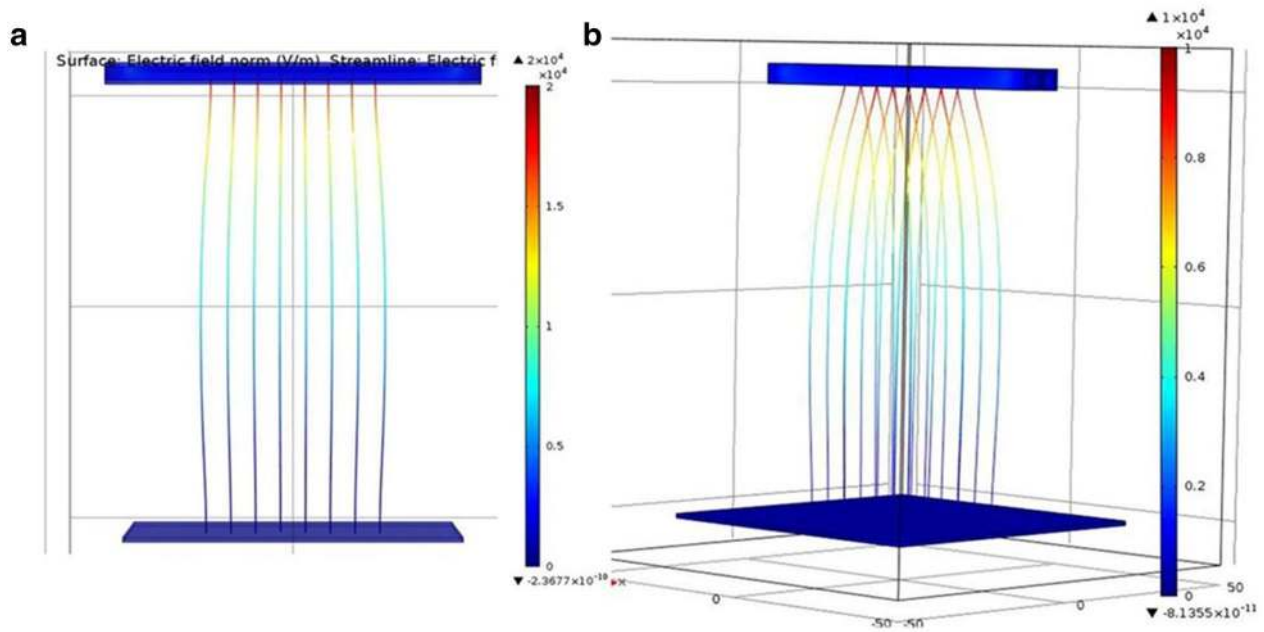

Fig. 3 Electric field streamlines showing repulsion in mulitjet electrospinning in **a** single tube and **b** dual tubes

Fig. 4 Electrospinning jets on tube nozzles, **a** 4 nozzles and **b** 8 nozzles architecture (φ indicates semi vertical angle). **c** Multi tube electrospinning using 2 tubes with 3 nozzles each showing Taylor cones, which are about to electrospin

Table 1 Semi-vertical-angles measured for 2, 4 and 8 nozzle architectures showing compression of electrospinning cones due to high density nozzles

Nozzle count	8	7	6	5	4	3	2	1
2							29.2°	22.8°
4					24.4°	20.6°	21.3°	22.7°
8	14.2°	13.0°	10.3°	10.7°	10.7°	12.1°	12.6°	14.6°

Nanofiber characterization

Figure 5 shows the scanning electron microscopy (SEM, JEOL 5700, JEOL Ltd.) images of electrospun nanofibers using TNE with a nozzle diameter (D_N) of 0.2 mm at different voltages and TCD conditions parameters for the 1 tube 2 nozzle TNE architecture. It is observed that nanofiber density decreases with increasing voltage and TCD. Moreover, the effect of the electric field generated electrostatic force on the electrospun nanofiber diameters is investigated and shown in Fig. 6 with the same TNE architecture as Fig. 5. At a nozzle diameter D_N of 0.2 mm, lower electric fields tend to give an evenly distributed

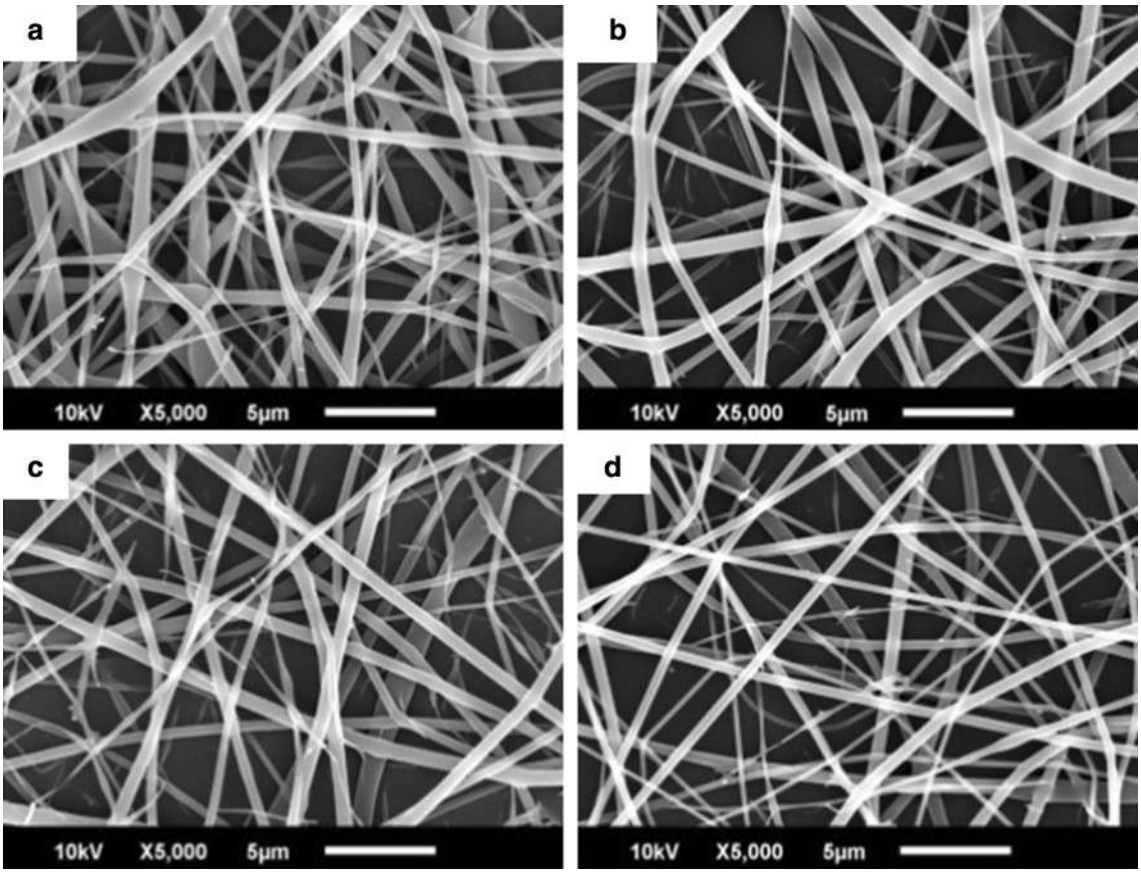

Fig. 5 Electrospun nanofibers collected at different operating conditions using the 1 tube and 2 nozzle TNE architecture with a nozzle diameter of 0.2 mm; **a** V = 12.5 kV, TCD = 10 cm (**b**) V = 12.5 kV, TCD = 12.5 cm (**c**) V = 15 kV, TCD = 10 cm (**d**) V = 15 kV, TCD = 12.5 cm [8]

diameter ranging from 200 to 500 nm as observed in Fig. 6a. As the electric field increases to 1.5 kV/cm, due to the higher voltage stretching the nanofibers thoroughly, the majority of nanofibers distributes around 200 nm as observed in Fig. 6c. Therefore, varying voltage can give varied distributions in the nanofiber diameter.

While the increased throughput of nanofibers can be achieved with a higher density of nozzles, the porosity of the stack is affected by the process parameters. The porosity of the nanofiber stacks is a crucial property which determines its effectiveness either in filtration, energy storage or tissue scaffold applications. The pore size and porosity of the nanofiber stack are measured by image software, ImageJ (National Institute of Health, USA). Table 2 shows the summary of porosity and pore size with different process parameters for the 1 tube 2 nozzle TNE architecture. Both porosity and pore size increases with increasing TCD as it allows for increased charge repulsion time of the nanofibers. The nozzle diameter can also affect the porosity of the nanofiber stacks. As the nozzle size becomes larger, it tends to produce nanofibers with larger diameters, thus resulting in the increase of the pore size of the nanofiber stacks.

Production and growth rates of TNE

Nanofiber throughput is calculated by the mass of nanofibers collected over a certain period of time. With the 2 nozzle architecture, 16.5 mg of SU-8 nanofibers is collected in a growth period of 16 min as tabulated in Table 3. This gives a mass throughput of 0.06 g/h per nozzle which is similar to that of the SNE technique [12]. Increasing the nozzle count on a single tube from 2 nozzles to 8 nozzles gives an eight-fold increase in production resulting in 0.46 g/h, which suggests that the throughput increases almost linearly with increases in nozzle count. While doubling the tube count on the 4 nozzle architecture, the production rate doubles to 0.49 g/h compared to that of the single tube of 0.25 g/h, the linear increase in throughput is not observed in the case of the 8 nozzle architecture from 0.46 to 0.75 g/h. It is in part attributed to the limited collector size, which

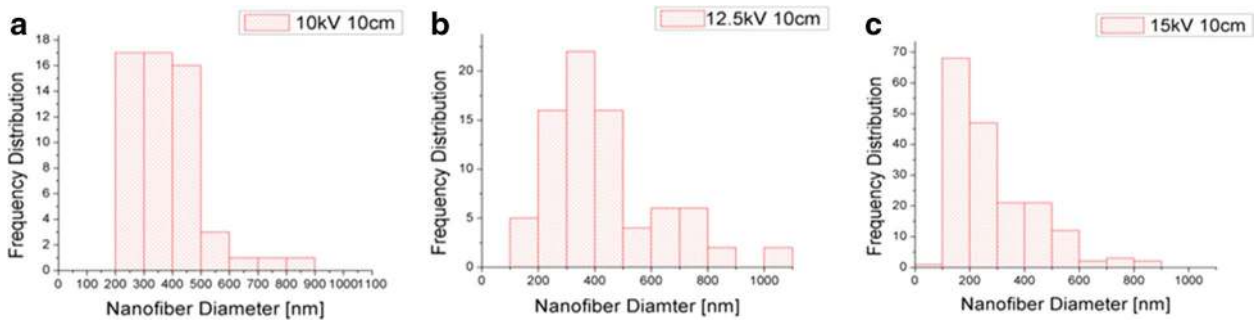

Fig. 6 Nanofiber diameter distribution histograms for the 1 tube and 2 nozzle TNE architecture with fixed TCD = 10 cm and varying operating voltage, **a** 10 kV, **b** 12.5 kV and **c** 15 kV

Table 2 Comparison of porosity and average pore size for the 1 tube 2 nozzle TNE architecture with different nozzle diameters and TCDs at constant voltage = 12.5 kV

TCD (cm)	7.5	10	12.5
Nozzle diameter = 0.2 mm			
Porosity (%)	29.1	31.0	35.3
Pore area (μm^2)	0.31	0.52	0.57
Nozzle diameter = 0.5 mm			
Porosity (%)	56.9	59.0	–
Pore area (μm^2)	0.28	2.46	–

could not include all the electrospun nanofibers as the nozzles are widely spread out.

Mean and standard deviation of the measured nanofiber stack height was calculated for the membrane over a distance of 1 cm. The TNE technique increases the throughput rate as expected from the reduced SVAs with the higher density of nozzles. The decrease in SVAs not only increases the throughput rate of the process, but also increase the directionality of the electrospun nanofibers. Due to the electrostatic repulsion of adjacent cones, electrospun nanofibers tend to be confined in a narrow space much like the electric field shaping due to an array of charged metallic rings [25].

Electric field shaping counters the bending instability of the nanofibers thus reducing the footprint of electrospun nanofibers on the collector. This decrease in footprint corresponds to an increase in thickness of the nanofiber stack as the volume of the produced nanofibers remains the same at a desired steady flow rate. Figure 7 shows the thickness of nanofiber stacks collected with an array of

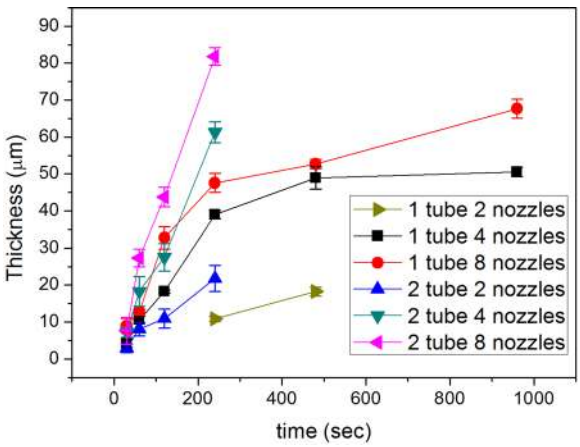

Fig. 7 Thickness of nanofiber stacks where *error bars* indicate stack height deviations

Table 3 Comparison of mass throughput for SU-8 based TNE with 2, 4 and 8 nozzles

Nozzle count	Nanofiber mass (mg)	Time of collection (min)	Mass throughput (g/h)
1 × 2	16.5	16	0.06
1 × 4	66	16	0.25
1 × 8	124	16	0.46
2 × 2	72	16	0.27
2 × 4	130	16	0.49
2 × 8	200	16	0.75

2, 4 and 8 nozzles equidistantly spaced at 0.5 cm apart in the single tube and double tube cases. The deposited nanofiber stack thickness increases with the increasing number of nozzle count as a higher nanofiber growth rate is achieved with higher directionality. In the case of the 2 tube 8 nozzle, 81.8 μm thick nanofiber stack is achieved at 240 s with an average deposition rate of 0.34 μm/s.

Using the 4 and 8 nozzles in the single tube architecture, a growth rate of 0.16 and 0.21 μm/s are obtained, respectively, using the multiple intermittent approach as shown in Table 3. The growth rate is observed to linearly increase until it starts to saturate at thicker collections at 480 s for both the 4 nozzle and 8 nozzle systems. Therefore, the growth rate is calculated in the linear growth region (<240 s) and given by the slope of the linear fitted curve. The saturation in height of the nanofibers is attributed to the electrostatic repulsion from the residual charge in the thicker stacked nanofibers.

Photolithographically patterned nanofibers

UV lithography allows the fabrication of patterns in the nanofiber matrix as shown in Fig. 8. Light diffusion is a common defect which corrupts the wave propagation through the nanofiber matrix. The red dotted lines in Fig. 8a, b delineate the original mask pattern and it is observed that the fabricated structures are larger than the mask patterns. Figure 8a, b compare the fabricated patterns with constant dosage for different heights of nanofibers. While both stacks are collected for 120 s, Fig. 8a, b are from 4 nozzles to give a stack height of 18.25 ± 0.41 μm, and from 8 nozzles to give a stack height of 32.74 ± 3.01 μm, respectively. When they are exposed with a constant dosage of 120 mJ/cm^2, the edge profile in Fig. 8b shows a thoroughly crosslinked nanofiber structure, while that in Fig. 8a shows overexposed nanofibers to give ring-like structures on the edges.

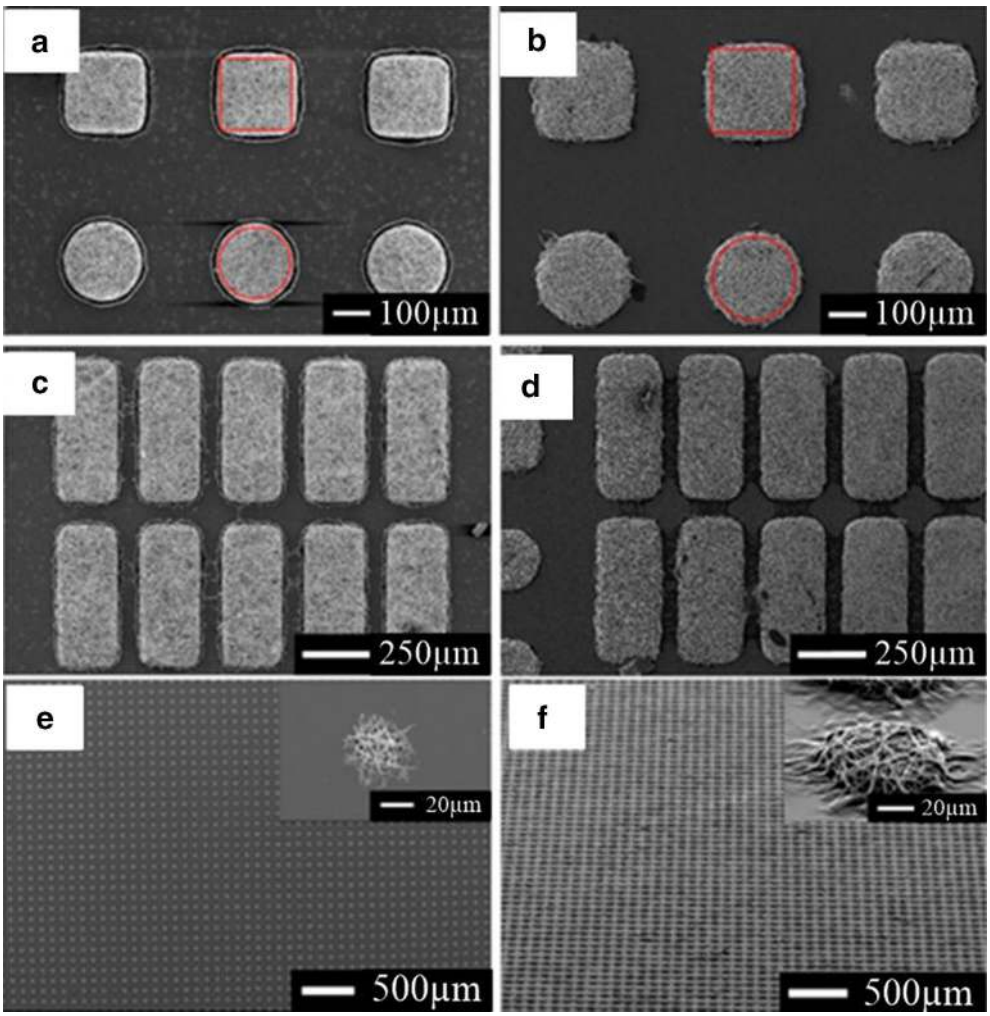

Fig. 8 SEM images of patterned nanofiber stacks with different stack heights of (**a**, **c**, **e**) 18.25 ± 0.41 μm, and (**b**, **d**, **f**) 32.74 ± 3.01 μm

Structures with diameters of 20 and 40 μm are patterned with SU-8 nanofibers as shown in the inset of Fig. 8e, f, respectively. Patterning resolution is limited by the light scattering effect due to the refractive index mismatch between SU-8 (n = 1.68) and air (n = 1) where the nominal nanofiber diameter (100–500 nm) and the wavelength of the UV source (*i*-line, λ = 365 nm) are in the similar range. With the uneven surface of SU-8 nanofibers, the large proximity gap between the mask and the photosensitive nanofibers results in pattern enlargement or deformation due to UV light refraction and diffraction. The previously reported oil-lithography patterning technique [26] can suppress this artifact to achieve high-aspect-ratio and high resolution microstructures.

Conclusions

Tube nozzle electrospinning (TNE) with multiple nozzles formed on an LDPE tube has been successfully demonstrated, which offers a superior production capability to the conventional SNE approach. The nonmetallic nozzles lower the electrostatic repulsion force between nanofibers which contributes to enhancing the growth rate of nanofibers. TNE with 8 nozzles on a plastic tube allows for the improved directionality of electrospun nanofibers, resulting in a low SVA of 12.28°. TNE with multiple nozzles shows the similar relationship of the nanofiber diameter to its operating parameters such as the nozzle diameter, the voltage and the TCD as the SNE system. The multiple intermittent growth technique is used to mitigate the effect of the accumulated charge and enhance the nanofiber growth rate. TNE demonstrates a high nanofiber collection rate of 0.46 and 0.75 g/h in the 1 × 8 and 2 × 8 nozzle architectures, respectively. An average deposition rate of 0.34 μm/s is obtained in TNE with the 2 × 8 nozzle architecture. Multi nozzle TNE shows potential of significant electrospinning time reduction which can ultimately contribute to reducing the manufacturing cost of nanofiber based devices. Lithographic patterning of thick SU-8 nanofibers without damaging the nanofibrous morphology is demonstrated. The result shows that TNE is an excellent nanofiber manufacturing approach with low nanofiber repulsion, high throughput production, high stack growth rate, and scalability.

Authors' contributions

SPF carried out the simulation, participated in its design, performed the experiments, and prepared the written material. PJ conceived of the study and design, and helped to draft the manuscript. DES participated in the experimental procedure concept and helped analyzing data. KTK participated in experimental setup and statistical analysis. YKY supervised the whole process including the design, experiment, analysis, and preparation of this manuscript. All authors read and approved the final manuscript.

Author details

[1] Electrical and Computer Engineering, University of Florida, 225 Larsen Hall, Gainesville, FL 32611-6200, USA. [2] Electrical and Electronic Engineering, Universidad Tecnológica de Bolívar, Cartagena, Colombia. [3] School of Science, Technology, Engineering, and Mathematics, University of Washington, Bothell, Washington 98011, USA.

Acknowledgements

The authors would like to thank Jessica Meloy and Dr. David Arnold for milling machine fabrication tips and training in the Interdisciplinary Microsystems Group (IMG Group), and David Hays and Al Ogden in Nanoscale Research Facilities at the University of Florida for assistance on the SEM measurements.

Competing interests

The authors declare that they have no competing interests.

Funding

This work is supported in part by NSF ECCS 1132413.

Received: 1 December 2016 Accepted: 13 January 2017
Published online: 27 January 2017

References

1. Huang Z (2003) A review on polymer nanofibers by electrospinning and their applications in nanocomposites. Compos Sci Technol 63(15):2223–2253
2. Teo W-E, Inai R, Ramakrishna S (2011) Technological advances in electrospinning of nanofibers. Sci Technol Adv Mater 12(1):013002
3. Fang J, Niu H, Lin T, Wang X (2008) Applications of electrospun nanofibers. Chin Sci Bull 53(15):2265–2286
4. Schreuder-Gibson H, Gibson P, Senecal K, Sennett M, Walker J, Yeomans W, Ziegler D, Tsai PP (2002) Protective textile materials based on electrospun nanofibers. J Adv Mater 34(3):44–55
5. Jao PF, Sun W, Yoon YK, Kim GJ (2010) Spatially controleld electrospun solif gradient nanofiebrs for guided spiral ganglion neuron culture. In Biomedical engineering society annual meeting, p 2
6. Jao PF, Machado M, Cheng X, Senior DE, Kim GJ, Ding D, Sun W, Yoon YK (2011) Fabrication of nanoporous membrane and its nonlithographic patterning using electrospinning and stamp-thru-mold (ESTM). In 2011 IEEE 24th International Conference on Micro Electro Mechanical Systems, pp 257–260
7. Jao PF, Cheng X, Kim GJ, Yoon YK (2012) Fabrication of a supercapacitor using an electrospun nanofiber based separator and carbon nanofiber electrodes. In The 12th international conference on micro and nanotechnology for power generation and energy conversion applications, p 4
8. Jao PF, Fang SP, David ES, Kim KT, Yoon YK (2012) Nanomanufacturing of large area carbon nanofibers using tube nozzle electrospinning (TNE), lithography and carbonization processes. In Electronic components and technology conference (ECTC), 2012 IEEE 62nd, pp 2075–2081
9. Yarin AL, Koombhongse S, Reneker DH (2001) Bending instability in electrospinning of nanofibers. J Appl Phys 89(5):3018
10. Luo CJ, Stoyanov SD, Stride E, Pelan E, Edirisinghe M (2012) Electrospinning versus fibre production methods: from specifics to technological convergence. Chem Soc Rev 41(13):4708–4735
11. Zhou F-L, Gong R-H, Porat I (2009) Mass production of nanofibre assemblies by electrostatic spinning. Polym Int 58(4):331–342
12. Theron SA, Yarin AL, Zussman E, Kroll E (2005) Multiple jets in electrospinning: experiment and modeling. Polymer 46(9):2889–2899
13. Tomaszewski W (2005) Investigation of electrospinning with the use of a multi-jet electrospinning head. Fibres Text East Eur 13(4):22–26
14. Dosunmu OO, Chase GG, Kataphinan W, Reneker DH (2006) Electrospinning of polymer nanofibres from multiple jets on a porous tubular surface. Nanotechnology 17(4):1123–1127
15. Varabhas JS, Chase GG, Reneker DH (2008) Electrospun nanofibers from a porous hollow tube. Polymer 49(19):4226–4229
16. Srivastava Y, Marquez M, Thorsen T (2009) Microfluidic electrospinning of biphasic nanofibers with Janus morphology. Biomicrofluidics 3(1):12801

17. Zhou F-L, Gong R-H, Porat I (2009) Polymeric nanofibers via flat spinneret electrospinning. Polym Eng Sci 49(12):2475–2481
18. Kumar A, Wei M, Barry C, Chen J, Mead J (2010) Controlling fiber repulsion in multijet electrospinning for higher throughput. Macromol Mater Eng 295(8):701–708
19. Kumar A, Asemota C, Padilla J, Invernale M, Otero TF, Sotzing GA (2008) Photopatterned conjugated polymer electrochromic nanofibers on paper. J Phys: Conf Ser 127(1):12014
20. Sundararaghavan HG, Metter RB, Burdick JA (2010) Electrospun fibrous scaffolds with multiscale and photopatterned porosity. Macromol Biosci 10(3):265–270
21. Kim G, Kim GJ, Yoon YK (2010) Lithographic patterning and carbonization of electrospun SU-8 nanofibers for a high capacity electrode. In Proceedings of solid stae sensors actuators and microsystems workshop, p 4
22. Kim GJ, Kim G, Yoon YK (2011) Fabrication of high energy density capacitors with micromachined carbon nanofiber electrocdes. In The 11th international conference on micro and nanotechnology for power generation and energy conversion applications, p 4
23. Steach JK, Clark JE, Olesik SV (2010) Optimization of electrospinning an SU-8 negative photoresist to create patterned carbon nanofibers and nanobeads. J Appl Polym Sci 118(1):405–412
24. Sharma CS, Sharma A, Madou M (2010) Multiscale carbon structures fabricated by direct micropatterning of electrospun mats of SU-8 photoresist nanofibers. Langmuir 26(4):2218–2222
25. Bellan LM, Craighead HG (2006) Control of an electrospinning jet using electric focusing and jet-steering fields. J Vac Sci Technol, B 24(6):3179–3183
26. Jao PF, Franca E, Fang S-P, Wheeler BC, Yoon YK (2015) Immersion lithographic patterning of electrospun nanofibers for carbon nanofibrous microelectrode arrays. J Microelectrochem Syst 24(3):703–715